Volume 65, Issue 1, 2021
Journal of Scientific Research
Institute of Science,
Banaras Hindu University, Varanasi, India.

Study of the Inactive Layer of sub-keV Point Contact Germanium Detector

M. K. Singh[*1], S. Karmakar[1], V. Singh[2,3], and H. T. Wong[4]

[1]Department of Physics, Institute of Applied Sciences and Humanities, G. L. A. University, Mathura - 281406, India. singhmanoj59@gmail.com*, shuvadeepk@gmail.com
[2]Department of Physics, School of Physical and Chemical Sciences, Central University of South Bihar, Gaya - 824236, India. venkaz@yahoo.com
[3]Department of Physics, Institute of Science, Banaras Hindu University, Varanasi – 221005, India. venkaz@yahoo.com
[4]Institute of Physics, Academia Sinica, Taipei - 11529, Taiwan. htwong@phys.sinica.edu.tw

Abstract: **The point contact germanium detectors are novel detector techniques offering kg-scale radiation sensors with sub-keV sensitivities. They have been used for light dark matter WIMPs searches and have potential applications in neutrino physics. Point contact germanium detectors are two types, one of them is n-type point contact and another one is p-type point contact germanium detector. In the p-type point-contact germanium detector there is an inactive layer due to which we have observed anomalous surface events, that increase the background in the sub keV region. While in n-type point contact germanium detector there is no inactive layer due to which we are free from the anomalous surface effect. To calculate the actual fiducial mass of the p-type point contact germanium detector we need to subtract the mass of the inactive layer for that we have to measure the thickness of the inactive layer. In this article, we focus on the anomalous surface event behavior coming due to the inactive layer in the p-type point-contact germanium detector and the process to measure the thickness of the inactive layer with using ^{133}Ba source and Monte Carlo simulation to calculate the actual fiducial mass of the p-type point-contact germanium detector.**

Index Terms: **Ionization p-type point-contact germanium detector, anomalous surface event behavior, measurement of inactive layer thickness, Dark matter search and low energy neutrino physics.**

I. INTRODUCTION AND PHYSICS MOTIVATION

Germanium detector with sub-keV sensitivities has been demonstrated as an efficient means to probe Weakly Interacting Massive Particles (WIMPs) [Soma, A. K. et al., 2017, Li, H. B. et al., 2014, Li, H. B. et al., 2013]. This novel detector is also adopted in the studies of neutrino-nucleus coherent scattering with reactor neutrinos [Soma, A. K. et al., 2017, Chen, J. W. et al., 2014]. The themes of the research program of the TEXONO (Taiwan EXperiment On NeutrinO) Collaboration are on the studies of low energy neutrino physics, such as neutrino-nucleus coherent scattering (NNCS), neutrino millcharge, charge radius, neutrino magnetic moments, and dark matter search at Kuo-Sheng Reactor Neutrino Laboratory (KSNL), Taiwan [Soma, A. K. et al., 2017]. P-type point-contact Germanium (pGe) detectors have excellent properties for the studies of low energy neutrino physics and search for dark matter candidates [Soma, A. K. et al., 2017]. A small area of the point-contact electrode, which can significantly reduce the internal capacitance, results in the reduction of low electronic noise and energy threshold [Soma, A. K. et al., 2017, Luke, P. N. et al., 1989]. The p-type point-contact Ge (pGe) detectors have an inactive layer at the surface caused by lithium diffusion [Soma, A. K. et al., 2017, H. B. et al., 2014, Aalseth, C. E. et al., 2013].

The events generated in the inactive layer will lead to a slow rise time pulse and an incomplete charge collection because of the very weak electric field in this region [Soma, A. K. et al., 2017, Li, H. B. et al., 2014, Li, H. B. et al., 2013, Aalseth, C. E. et al., 2013, Aguayo, E. et al., 2013, Burns, P. A. et al., 1990]. The events interacting in this inactive layer region are not providing the primary energies that are deposited in the detector, therefore, we must have to discriminate these events from the bulk events by using proper efficiency corrections [Li, H. B. et al., 2014]. After calculating the thickness of the inactive layer we can precisely measure the fiducial mass of the detectors, which is one of the important parameters of any detector for rare events search experiments [Soma, A. K. et al., 2017]

II. EXPERIMENTAL OVERVIEW

A schematic diagram of the data readout with a Ge detector is shown in figure 1. First of all the signals from the germanium crystal sensor are amplified by the front end JFET, which is

*Corresponding Author

DOI: 10.37398/JSR.2021.650130

located very close to the germanium diode. Subsequently, this output signal is fed to the reset preamplifier, placed ~30 cm away from the detector [Soma, A. K. et al., 2017]. The schematic drawing of the preamplifier output signal as observed on an oscilloscope is shown in figure 2. The scales shown are typical, while the exact scales vary for different germanium detectors [Soma, A. K. et al., 2017]. The output signals of the preamplifier are fed to the shaping amplifier and fast timing amplifier, to obtain the energy and rise-time information, respectively [Soma, A. K. et al., 2017]. The small falls event as mentioned in figure 2, are the real physics events while the reset line shows that the time when the detector is not taking the signal. The symbol Δt^- and Δt^+ gives the information of the previous and next reset signal for those events. The output of the timing and shaping amplifiers are shown in figure 3a and figure 3b respectively, for various samples of events [Soma, A. K. et al., 2017, Li, H. B. et al., 2014, Li, H. B. et al., 2013]. The discriminator output provides the trigger instant for data acquisition (DAQ). We used 60 MHz and 200 MHz Flash Analog-to-Digital Converters (FADC), to digitize the pulses from the shaping and timing amplifiers, respectively [Soma, A. K. et al., 2017].

In this article, we will follow the notations as reported in our earlier works [Soma, A. K. et al., 2017, Li, H. B. et al., 2014, Li, H. B. et al., 2013] where CR and AC denote the cosmic-ray veto systems and anti-Compton detector respectively, while the superscript +(-) corresponds to coincidence (anti-coincidence) with the Ge detector signals. The events sample $CR^- \otimes AC^- \otimes B$ denotes the Neutrino- and WIMP-induced candidates [Soma, A. K. et al., 2017, Li, H. B. et al., 2014, Li, H. B. et al., 2013].

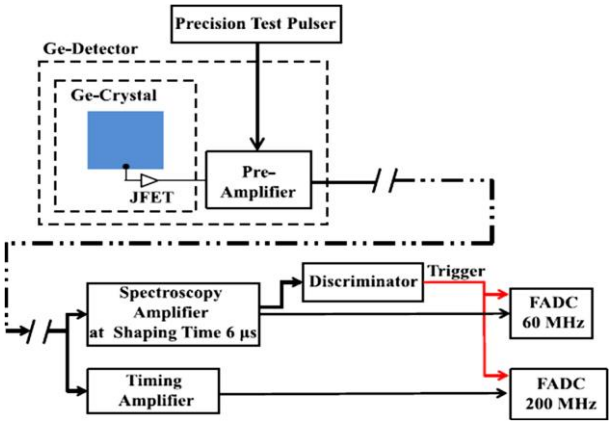

Fig. 1. Schematic layout of the DAQ system for the Ge detector [Soma, A. K. et al., 2017].

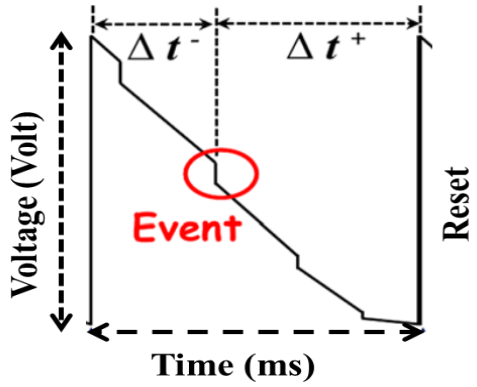

Fig. 2. Schematic drawing of the preamplifier output signals as seen on the oscilloscope [Soma, A. K. et al., 2017]. The scales are typical

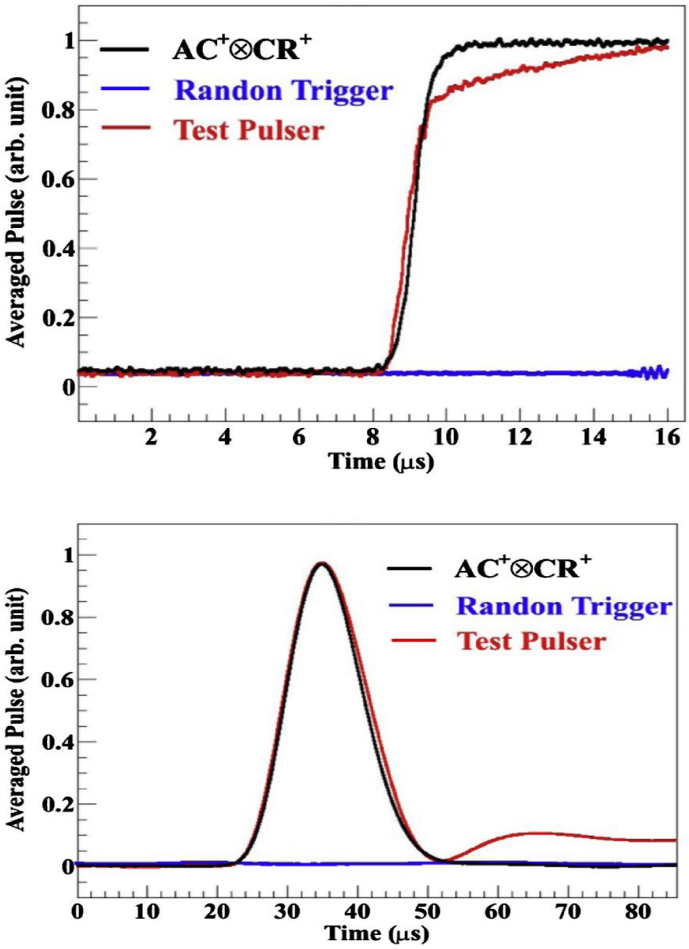

Fig. 3. The output signals of the (up) Timing Amplifier and (down) Shaping Amplifier for various samples of event [Soma, A. K. et al., 2017, Li, H. B. et al., 2014, Li, H. B. et al., 2013].

III. Anomalous Surface Events In p-Type Point Contact Germanium Detectors

1) Germanium detector geometry

The TEXONO detector was custom-designed, and fabricated by Canberra. The germanium crystal, has a diameter of 60 mm, a height of 60 mm, is encapsulated in an Oxygen-Free-High-Conductivity (OFHC) copper cryostat. The copper thickness at

the endcap side opposite the point contact is 1.5 mm and at the side is 2.0 mm. The distance between the endcap and the germanium crystal is 3.0 mm and there is no other material but vacuum between them. At the side, there are some supports, foils, and screws made of OFHC copper, lead, and brass. The point contact is at the bottom of the crystal and connected to a brass pin to read out the signals. The schematic geometry of the Ge detector is shown in figure 4a while the simulated schematic geometry of the Ge detector is shown in figure 4b.

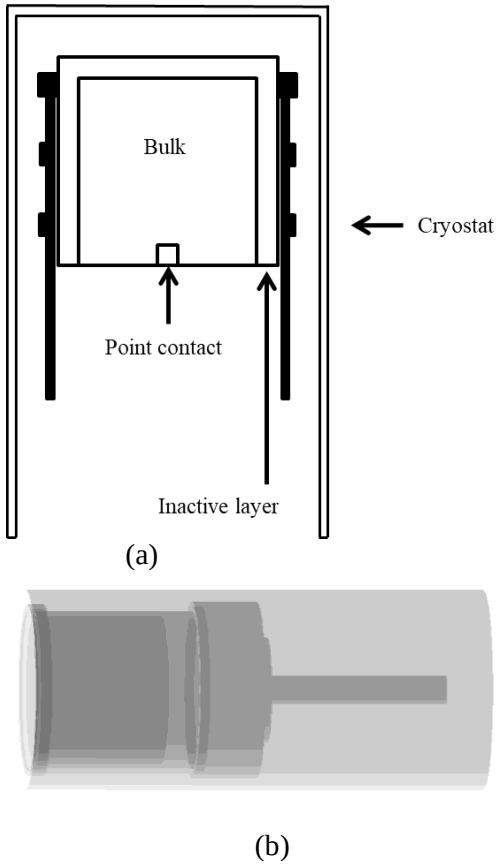

Fig. 4. (a) The layout of the Ge detector. The dimensions of the point contact and dead layer are not shown to scale. (b) The simulated schematic diagram of Ge detector.

2) Physics origin of surface and bulk events

The entire volume of the pGe detector can be distinguished into two main parts, one of them is the surface part (inactive layer), where no charge or only part of the charge is collected by the electrodes, and another one is the bulk part, in which all charge produced is fully collected by the electrodes [Soma, A. K. et al., 2017, Li, H. B. et al., 2014, Li, H. B. et al., 2013, Aalseth, C. E. et al., 2013]. The schematic diagram of a typical pGe sensor including the transition layer is shown in figure 5a.

The crystal is made of p-type germanium and the outer surface electrode is at positive high voltage towards which the electrons are drifted [Li, H. B. et al., 2014]. The small central contact electrode is at zero-potential from which electrical signals are extracted [Soma, A. K. et al., 2017, Li, H. B. et al., 2014, Li, H. B. et al., 2013]. The outer surface electrode is fabricated by lithium diffusion [Soma, A. K. et al., 2017].

The signals generated in the surface part have a much slower rise time and an incomplete charge collection while in bulk part have a fast rise time and complete charge collection, because electron-hole pairs produced by radiations at the surface (S) layer are subjected to a weaker drift field than those in the crystal bulk region (B) [Soma, A. K. et al., 2017, Li, H. B. et al., 2014]. Hence, the characteristics of surface-events have only partial charge collection and slower rise-time.

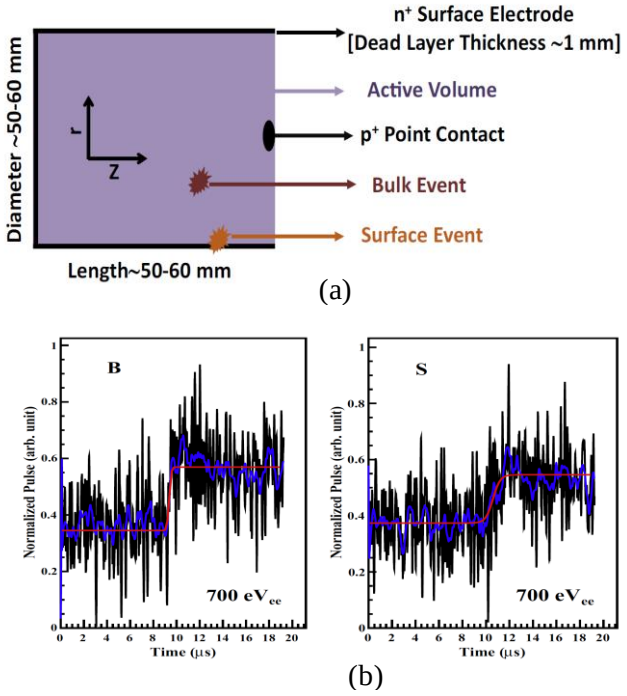

Fig. 5. (a) Schematic crystal configurations of the pGe detectors, (b) Timing amplifier signals at 700 eV from bulk and surface region of pGe showing the raw (black) and smoothed (blue) pulses, together with the best-fit functions (red) [Li, H. B. et al., 2014].

These anomalous surface events severely affect the low energy background [Soma, A. K. et al., 2017, H. B. et al., 2014]. Therefore the identification of the surface events and the knowledge of efficiency factors become crucial to fully exploit the sub-keV sensitivities of the pGe detector [Soma, A. K. et al., 2017, Li, H. B. et al., 2014, Li, H. B. et al., 2013]. The thickness of the surface layer for the pGe detector can be measured by the comparison of simulated and observed intensity ratios of γ-peaks from a ^{133}Ba source [Aguayo, E. et al., 2013]. The thickness measurement process is described in detail in section 4.

3) Bulk and surface event differentiation

The typical pulse shape of timing-amplifiers (TA) for B/S-events at low (700 eV) energy is shown in figure 5b. The rise-

time (τ) of the TA-signal is parametrized by the hyperbolic tangent function,

$$F(t)=\frac{A_0}{2}\tanh\left(\frac{t-t_0}{\tau}\right)+P_0. \quad (1)$$

Where, P_0, t_0, and A_0 are pedestal offset, timing offset, and amplitude, respectively. The values of P_0 and A_0 are evaluated from the TA-pulses prior to the transition edge and through the difference of the asymptotic levels, respectively [Li, H. B. et al., 2014]. First of all, we smoothed the raw TA-pulses by using the Softies-Kola filter [H. B. et al., 2014] and fit the pulse using equation (1) with (τ, t_0) as free parameters. These fit results are then used as input values for another fit of the same function directly on the raw pulses [Li, H. B. et al., 2014]. The raw FADC signals overlaid with smoothed and best-fit functions are shown in figure 5b.

The scatter plot of $\log_{10}[\tau]$ versus measured energy (T) for the $AC^-\otimes CR^-$ (i.e. single sited) events is shown in figure 6. From figure 6 it is clear that the events with τ more than a selected cut-value τ_0 (= 1.23 μs) are categorized as surface events and events less than τ_0 value are categorized as bulk events, respectively [Soma, A. K. et al., 2017, H. B. et al., 2014, H. B. et al., 2013]. A small fraction (<8%) of events at low energy (i.e., sub-keV region) fails the fitting procedures. Therefore we excluded these events from the subsequent analysis [Li, H. B. et al., 2014]. The signal efficiency of these excluded events is measured from the survival probability of the doubly-tagged $AC^+\otimes CR^+$ (high energy muons) sample events, which is more than 80% [Li, H. B. et al., 2014].

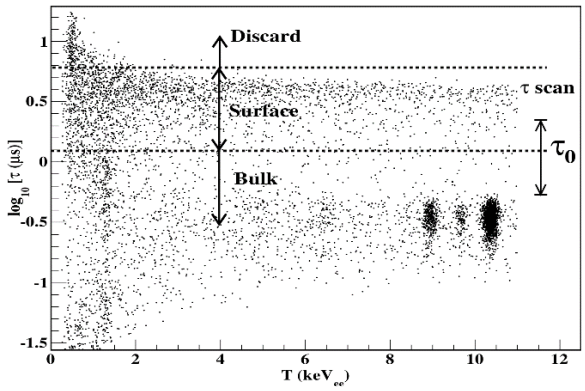

Fig. 6. The τ distribution versus T scatter plot for the $AC^-\otimes CR^-$ events.

To calculate the efficiency of surface/bulk events cut, we used (I) Surface-rich events with ^{241}Am and ^{137}Cs gamma-ray sources and (II) Bulk-rich events with cosmic-ray induced fast neutrons as-described in Ref. [Li, H. B. et al., 2014].

IV. ESTIMATION OF THE THICKNESS OF THE INACTIVE LAYER

1) Experimental result

^{133}Ba isotope is an excellent source to measure the inactive layer's thickness of the pGe detector because it has several photoelectron peaks as shown in table 1 [Khazov, Y. et al., 2011]. The basic idea behind this is that the different energy gamma rays have different attenuation lengths in a Ge crystal. Lower energy photons are more likely to interact in the inactive layer compared to higher energy photons. Therefore, the thickness of the dead layer can be derived by comparing a higher energy photoelectron peaks to the 81 keV photoelectron peak of the ^{133}Ba source [Khazov, Y. et al., 2011, Jiang, H. et al., 2016].

Table 1. γ - ray energies with their intensities of ^{133}Ba isotope [Khazov, Y. et al., 2011].

Energy (keV)	Intensity (%)	Energy (keV)	Intensity (%)
53.16	2.14	276.40	7.16
79.61	2.65	302.85	18.34
81.00	32.95	356.01	62.05
160.61	0.64	383.85	8.94
223.24	0.45		

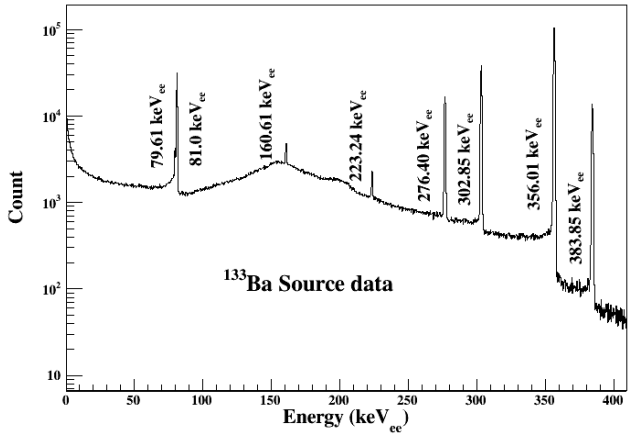

Fig. 7. Observed energy spectrum of ^{133}Ba isotope with pGe detector.

For this study, we have used ^{133}Ba isotope having an intensity of 1.139 μCi and the data have been taken for ~10 hours. The energy spectrum of ^{133}Ba isotope with pGe detector taken at the TEXONO home laboratory is shown in figure 7. In this spectrum, there are seven explicit photoelectron peaks at energies 81 keV, 160.6 keV, 223.2 keV, 276.4 keV, 302.8 keV, 356 keV and 383.8 keV. The 160.6 keV and 223.2 keV photoelectron peaks of the ^{133}Ba isotope are not used in the thickness measurement because these peaks are significantly smaller than the rest of the peaks [Khazov, Y. et al., 2011, Jiang, H. et al., 2016].

The two peaks at the energies 79.6 keV and 81 keV of the ^{133}Ba isotope spectrum are too close to each other, therefore two Gaussian functions and a linear function are applied for the fitting as shown in figure 8a. The fit result of the 356 keV photoelectron peak is shown in figure 8b. A Gaussian function and a linear function are used to describe the peak region. The peak area are calculated by using the equation as below,

$$A = \sqrt{2\pi}\sigma H/W, \quad (2)$$

Where, A represents the peak area, σ refers to the FWHM of the Gaussian fitting function, H refers to the peak height and W represents the width of the energy bins.

By using the fit results of figure 8 (a&b), the ratios of different photoelectron peaks are calculated and are normalized to the area under the peak at 81 keV. The results are shown in table 2.

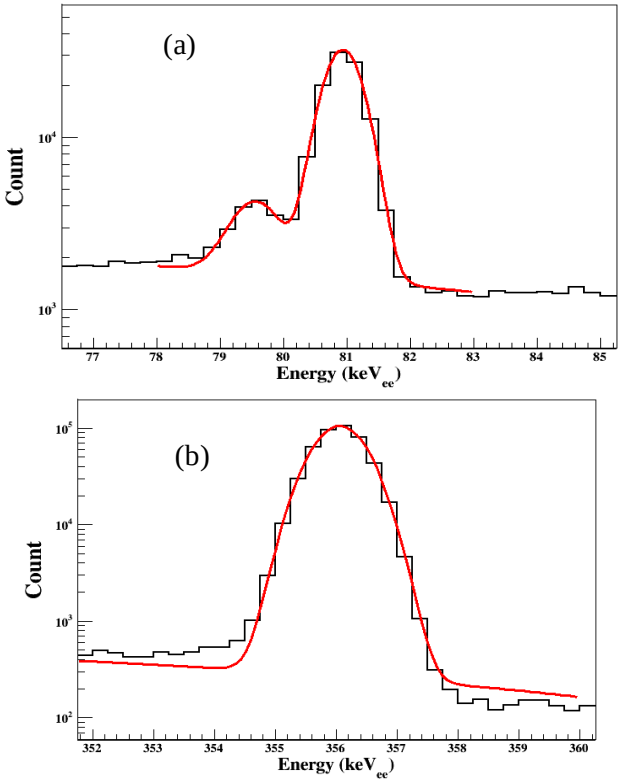

Fig. 8. (a) The Gaussian-linear function fitting on the peaks of 79.6 keV and 81 keV, (b) and on the peak of 356 keV of the ^{133}Ba spectrum.

Table 2. Different energy peak ratios of ^{133}Ba isotope.

Energy Peak (keV)	Energy peak ratio with that of 81 keV
276.40	0.518 ± 0.003
302.85	1.238 ± 0.006
356.01	3.655 ± 0.017
383.85	0.491 ± 0.003

2) Simulation data analysis

Geant4 version 9.5 was used to simulate the initial interaction of the gamma rays from ^{133}Ba isotope with the pGe detector. In the simulation, the inactive layer thickness was varied from 0.2 mm to 2.0 mm to get different simulated results of the ^{133}Ba isotope. The surface events with continuous energy deposition cannot affect the ratios of areas under different photoelectron peaks, due to which only the bulk events were considered in the simulation [Soma, A. K. et al., 2017, Li, H. B. et al., 2013, Aguayo, E. et al., 2013, Jiang, H. et al., 2016]. The simulated energy spectrum of the ^{133}Ba isotope is shown in figure 9.

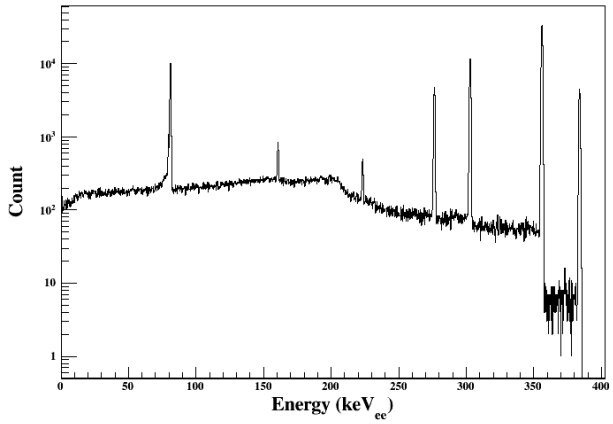

Fig. 9. The simulated energy spectrum of the ^{133}Ba isotope.

Figure 10, shows the ratio of the number of events in the 356 keV photoelectron peak to the 81 keV photoelectron peak for different thicknesses of the inactive layer. A quadratic fitting function provides a good description of the simulation results [Khazov, Y. et al., 2011, Jiang, H. et al., 2016]. The horizontal band/line shows the ratio of area under 356 keV photoelectron peak to that of 81 keV photoelectron peak with 1σ error bar that was determined from the experimental data (shown in table 2), while the vertical band/line indicates the intersection point of simulation and measured data with 1σ error bar, which shows the thickness of inactive layer corresponding to 356 keV peak [Khazov, Y. et al., 2011, Jiang, H. et al., 2016]. With the help of this technique, the rest of the photoelectron peaks of ^{133}Ba isotope are evaluated and the results are tabulated in table 3.

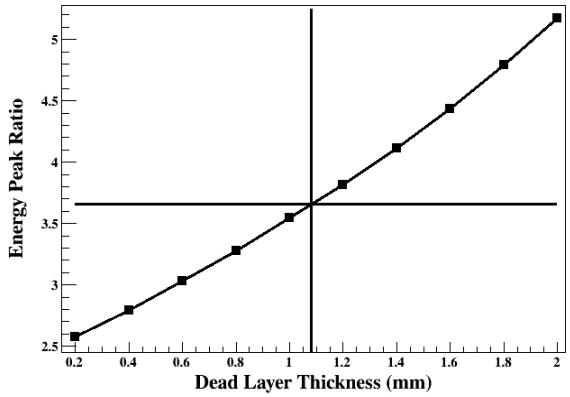

Fig. 10. Estimation of the inactive layer thickness of the pGe detector corresponds to a 356 keV photoelectron peak of ^{133}Ba isotope. The points are from the simulation data analysis, providing the ratios of the number of events in the 356 keV and 81 keV photoelectron peak of ^{133}Ba isotope. The horizontal band/line shows the ratio of 356 keV photoelectron peak to the 81 keV photoelectron peak with 1σ error bar that was measured

by the experimental data (shown in table 2) while the vertical band/line indicates the intersection point of simulation and measured data drawn with 1σ error bar.

Table 3. The calculated thicknesses of inactive layer with statistical uncertainties for different energy peaks.

Energy peaks / 81 keV	Thickness of inactive layer (mm)	Statistical uncertainty (mm)
276.40	1.231	0.031
302.85	1.173	0.029
356.01	1.085	0.024
383.85	1.028	0.025

The statistical uncertainty of these results, obtained by peak area using equation (2), can be calculated in two steps. In the step first, we used equation (3) for calculating the statistical uncertainty.

$$\sigma_s = \sigma\left(\frac{Q_1}{Q_2}\right) = \frac{H_1}{H_2}\frac{\sigma_1}{\sigma_2}\sqrt{\left(\frac{\sigma_{H_1}^2}{H_1^2} + \frac{\sigma_{\sigma_1}^2}{\sigma_1^2} + \frac{\sigma_{H_2}^2}{H_2^2} + \frac{\sigma_{\sigma_2}^2}{\sigma_2^2}\right)} \qquad (3)$$

Where, σ_s corresponds to the statistical uncertainties of peak ratios, Q_i, H_i, and σ_i correspond to the peak area, peak height, and sigma value of the photoelectron peak i (i = 1,2). The statistical uncertainties calculated by this technique are shown in table 2. In the second step, the uncertainties of the different energy peak ratios calculated by equation (3) were added to the experimental results. The width of the horizontal band/line shown in figure 10, represent the calculated statistical uncertainty. The width of the vertical band/line drawn from the two intersections of the measured statistical uncertainties of the horizontal band/line represents the statistical uncertainty of the thickness of the inactive layer. The statistical uncertainty obtained by this method is shown in table 3.

The central value and statistical uncertainty of the inactive layer thickness were calculated using the weighted average method [Khazov, Y. et al., 2011, Jiang, H. et al., 2016]. The estimated value of the inactive layer thickness of 900g pGe detector having a diameter of 60 mm and a height of 60 mm is 1.115 ± 0.013 mm. Adopting the above-mentioned method, we estimated the thickness of inactive layer 1.013 ± 0.012 mm for 500g pGe detector having a diameter of 50 mm and a height of 50 mm, respectively.

Conclusion

In this article, we reported the measured value of the inactive layer thickness for two different detectors 900g and 500g used in the TEXONO experiment for low energy neutrino physics and dark matter search. In this study, a ^{133}Ba isotope was used as a source to measure the thickness of the inactive layer of the pGe detector. The measured value of the inactive layer thickness is ~ 1.115 ± 0.013 mm for a 900g pGe detector having a diameter of 60 mm and a height of 60 mm and 1.013 ± 0.012 mm for a 500g pGe detector having a diameter of 50 mm and a height of 50 mm. The measured value of the inactive layer is important to calculate the fiducial mass of the Ge detector.

After knowing the thickness of the inactive layer by using the above-mentioned method, we have used the detector dimension, the density of crystal, and the thickness of inactive layer to calculate the mass of the inactive layer which are 60g and 20 g for the 900g pGe and 500g pGe detector respectively [10], while the detector mass 900g and 500g are provided by Company which is before the inactive layer mass subtraction. Therefore after subtracting the mass value of the inactive layer from the given mass of the detector, we find the fiducial mass of 900g pGe and 500g pGe detectors are 840g and 480g respectively and which is further used to normalize the energy spectrum of the pGe detector and obtain the physics data for low energy neutrino physics as well as dark matter searches.

Acknowledgment

The research programs and results presented in this article are from the efforts of the TEXONO Collaboration consisting of groups from Taiwan (Academia Sinica, KuoSheng Nuclear Power Station), China (Tsinghua University, Institute of Atomic Energy, Nankai University, Sichuan University), India (Banaras Hindu University, G. L. A. University) and Turkey (Middle East Technical University, Dokuz Eyll University). The authors are grateful to the contributions from all collaborators.

References

Soma, A. K. et al., (2017). Characterization and performance of germanium detectors with subkeV sensitivities for neutrino and dark matter experiments. Nuclear Instruments and Methods in Physics Research A, 836, 67-82.

Li, H. B. et al., (2014). Differentiation of bulk and surface events in p-type point-contact germanium detectors for light WIMP searches. Astroparticle Physics, 56, 1-4

Li, H. B. et al., (2013). Limits on Spin-Independent Couplings of WIMP Dark Matter with a p-Type Point-Contact Germanium Detector. Physical Review Letter, 110, 261301(1-5).

Chen, J. W. et al., (2014). Constraints on millicharged neutrinos via analysis of data from atomic ionizations with germanium detectors at sub-keV sensitivities. Physical Review D, 90, 011301(R) (1-5).

Luke, P. N. et al., (1989). Low capacitance large volume shaped-field germanium detector. IEEE Transactions on Nuclear Science, 36, 926-930.

Aalseth, C. E. et al., (2013). CoGeNT: A search for low-mass dark matter using p-type point contact germanium detectors. Physical Review D, 88, 012002 (1-20).

Aguayo, E. et al., (2013). Characteristics of signals originating near the lithium-diffused N+ contact of high purity germanium p-type point contact detectors. Nuclear Instruments and Methods in Physics Research A, 701, 176-185.

Burns, P. A. et al., (1990). Needle beam studies of HPGe Detectors for photon efficiency calibration from 6 to 25 keV. Nuclear Instruments and Methods in Physics Research A, 286, 480-489.

Khazov, Y. et al., (2011). Nuclear Data Sheets. 112, 935.

Jiang, H. et al., (2016). Measurement of the dead layer thickness in a p-type point contact germanium detector. Chinese Physics C, 40(9), 096001 (1-7).

***